https://doi.org/10.5194/egusphere-2026-2055
Preprint. Discussion started: 15 April 2026

RADEM observations of the Van Allen belts during the JUICE Lunar-Earth Gravity Assist

Marco Pinto[1], André Rodrigues[1], Elias Roussos[2], Daniel Schmid[3], Martin Volwerk[3], Stavros Kotsiaros[4], Patrick Brown[5], Michele Dougherty[5], Luísa Arruda[1], and Olivier Witasse[6]

[1]LIP, Laboratory for Instrumentation and Experimental Particle Physics, Av. Prof. Gama Pinto 2, 1649-003 Lisbon, Portugal
[2]Max Planck Institute for Solar System Research, Justus-von-Liebig-Weg 3, 37077 Göttingen, Germany
[3]Space Research Institute, Austrian Academy of Sciences, Schmiedlstraße 6, A-8042 Graz, Austria
[4]European Space Agency (ESA), European Space Astronomy Centre (ESAC), Camino Bajo del Castillo s/n, 28692 Villanueva de la Cañada (Madrid), Spain
[5]Department of Physics, Imperial College London, London SW7 2AZ, UK
[6]European Space Agency (ESA), European Space Research and Technology Centre (ESTEC), Keplerlaan 1, 2201 AZ Noordwijk, the Netherlands

Correspondence: Marco Pinto (mpinto@lip.pt)

Abstract. On 19–20 August 2024, the European Space Agency (ESA) Jupiter Icy Moons Explorer (JUICE) mission performed the first ever Lunar–Earth Gravity Assist (LEGA) manoeuvre. The mission was launched on April 14, 2023, and is currently on an 8-year interplanetary cruise to the Jovian system. It is equipped with the RADiation-hard Electron Monitor (RADEM), a facility instrument designed to measure the most energetic particle populations (electrons, protons and ions) in the Jovian environment where JUICE will operate. During LEGA, JUICE crossed the Van Allen belts, providing a unique opportunity to evaluate the in-flight response of RADEM and to optimize its configuration for the Jupiter phase. In this paper, we report RADEM observations of the Van Allen belts, showing clear sensitivity to trapped electrons and protons. We also discuss how the Earth-flyby geometry, including pitch-angle effects, influenced the measurements and the implications for future operations. The observations also demonstrate that while RADEM is a facility instrument, it has the potential to enhance the scientific return of the JUICE mission by monitoring a key energy range in Jupiter's radiation belts that no other instrument on JUICE is covering.

1 Introduction

The Jupiter Icy Moons Explorer (JUICE, Grasset et al., 2013; Boutonnet et al., 2026) mission is the first L-class mission of the European Space Agency (ESA) Cosmic Vision program. JUICE will study the Jovian system and its three largest icy moons, Callisto, Ganymede, and Europa. It will make detailed observations of Jupiter's atmosphere (Fletcher et al., 2023), the magnetospheres of Jupiter and Ganymede (Masters et al., 2025), and the geology of the moons (Tosi et al., 2024; Denk et al., 2026; Van Hoolst et al., 2024). JUICE was launched on April 14, 2023, and is expected to enter Jupiter orbit in July 2031. To do so, it executed the first-ever Lunar–Earth Gravity Assist (LEGA) on August 19–20, 2024 (Dietz et al., 2026), and a Venus gravity assist on August 31, 2025. Two additional Earth gravity assists are planned for 2026 and 2029.

https://doi.org/10.5194/egusphere-2026-2055
Preprint. Discussion started: 15 April 2026

Over the course of its operations, the mission will encounter an extremely hazardous radiation environment in the form of energetic charged particles. These can be separated into three main sources: galactic cosmic rays (GCR; e.g. Potgieter, 2013)-extremely energetic particles (predominantly ions) accelerated outside the solar system; solar energetic particles (SEPs) emitted from the Sun and/or accelerated in coronal mass ejections (e.g. Reames, 2013; Lario et al., 2022); and energetic particles trapped in planetary magnetic fields such as those on Earth and Jupiter (e.g. Kanekal and Miyoshi, 2021; Kollmann et al., 2018; Nénon et al., 2022). These particles produce acute effects in electronics, commonly known as single-event effects (Oldham and McLean, 2003), and cumulative ionizing (Dodd and Massengill, 2003) and non-ionizing radiation damage (Srour et al., 2003), reducing semiconductor performance and lifetime.

Jupiter's radiation belts contain extremely energetic populations of both electrons and protons, with particle intensities that exceed those observed in Earth's magnetosphere by several orders of magnitude (Van Allen et al., 1975). In particular, ultra-relativistic electrons with energies above 10 MeV are present in the Jovian inner magnetosphere (Bolton et al., 2002). Their intensity close to the planet is so high that they can be observed remotely from Earth in the form of synchrotron radiation. But even at the distances that JUICE will operate, outside Europa's orbit, the intensities of electrons above 1 MeV are several orders higher than those in the most hazardous region of Earth's Van Allen belts. These electrons are a major contributor to the total ionizing dose accumulated by spacecraft systems and can also cause deep dielectric charging, posing a significant risk to electronic components and solar arrays through cumulative degradation and internal electrostatic discharge.

Despite their importance for spacecraft design and mission operations, the highest-energy electron populations in Jupiter's radiation belts remain comparatively poorly constrained and several papers have addressed the importance of better understanding their structure and dynamics (Roussos et al., 2022; Clark et al., 2026). Previous missions, including Galileo (Williams, 2004) and Juno (Bolton et al., 2017), have provided valuable in situ observations of the Jovian radiation environment. However, continuous measurements of electrons in the 10–100 MeV range remain limited. Existing radiation environment models rely on extrapolations from lower-energy measurements.

The JUICE spacecraft carries a suite of ten scientific instruments designed to investigate the Jovian system and its moons. Plasma and particle measurements are performed by the Particle Environment Package (PEP; Barabash et al., 2016). Within this suite, the Jovian Energetic Electrons (JoEE) sensor is designed to characterize the Jovian energetic-electron population up to energies of about 8 MeV. As a result, the ultra-relativistic electrons that dominate the spacecraft radiation dose lie outside the primary measurement range of JoEE.

To address this gap, JUICE carries the RADiation-hard Electron Monitor (RADEM; Hajdas et al., 2025; Pinto et al., 2026), a dedicated facility instrument designed to detect very energetic particles throughout the mission, help identify the causes of anomalies, and support operations planning. It will also perform scientific measurements that support the characterization and modelling of Jupiter's radiation belts.

RADEM operates continuously during the JUICE cruise phase and has already measured tens of SEP events (Pinto et al., 2026). SEP measurements have been used to validate and calibrate RADEM's proton response (Rodríguez-García et al., 2025). Isolating the electron response is more difficult because the electron flux during SEPs is much lower than the proton flux and

https://doi.org/10.5194/egusphere-2026-2055
Preprint. Discussion started: 15 April 2026

RADEM was designed to operate in much more intense electron environments. During LEGA, JUICE crossed Earth's radiation belts, providing a unique opportunity to evaluate RADEM's sensitivity to electrons.

2 RADEM

RADEM consists of four detector heads: the Electron Detector Head (EDH), Proton Detector Head (PDH), the Heavy Ion Detector Head (HIDH), and the Directional Detector Head (DDH, Pinto et al., 2019). They were designed to measure electrons from 300 keV to 40 MeV, protons from 5 MeV to ∼250 MeV, ions from helium to oxygen, and electron angular distribution from 300 keV to 2 MeV, respectively (Pinto, 2019). The EDH, PDH and HIDH are dE/dX-dE silicon-stack detectors with relatively narrow fields-of-view (FOVs), 15 ° for the EDH, 20 ° for the PDH and 40 ° for the HIDH. This ensures the detectors can operate in the high-flux environment present in the Jovian system. Stack detectors measure particle energies based on how far in the stack they have traveled and distinguish between particle types based on their deposited energy profile (Pinto, 2019). The DDH is a single copper collimator with 28 holes corresponding to 28 viewing directions. These are split into 4 zenithal angles (0 ° - one sensor, 22.5 ° - 9 sensors, 45 ° - 9 sensors, 67.5 ° - 9 sensors). The active region consists of a single silicon plane sensor with 28 pixels corresponding to the projected area of each collimator hole. Three obscured pixels are also present to monitor penetrating particles, which represent the main background of the detector.

RADEM's detectors are highly configurable. They can be sensitive to different particle species and energies depending on their settings. For example, the PDH, EDH and DDH can switch their sensitivity from electrons to protons and vice versa. During LEGA, the PDH was configured in multiple coincidence mode to measure proton spectra (see Pinto et al. (2026) for more details). The EDH was in single configuration mode to maximize its geometric factor.

RADEM's science data is organized into five variables: PROTONS, ELECTRONS, HEAVY_IONS, DD, and CUSTOM. The first four correspond to detection bins associated with the PDH, EDH, HIDH, and DDH, respectively. CUSTOM contains a combination of PDH and EDH detection bins. While the HIDH and DDH also made measurements during the flyby, in this manuscript we focus on the EDH and PDH only.

The sensitivity of each detection bin analysed in this manuscript is described in Table 1. Their response functions are shown in Fig. 1. Notice that the ELECTRONS detection bins, corresponding to EDH signal processing can be contaminated by high-energy protons (>70 MeV). Low-energy protons (7–8 MeV) may also contaminate the ELECTRONS 1 channel. While these particles represent a large background during SEPs, in the Van Allen belts, the two particle populations are well separated, especially in the outer belt where electrons dominate. This was one of the main goals of RADEM during LEGA: to assess its in-flight response to electrons.

More information about RADEM's design, working principle, and response functions can be found in Hajdas et al. (2025); Pinto et al. (2026).

https://doi.org/10.5194/egusphere-2026-2055
Preprint. Discussion started: 15 April 2026

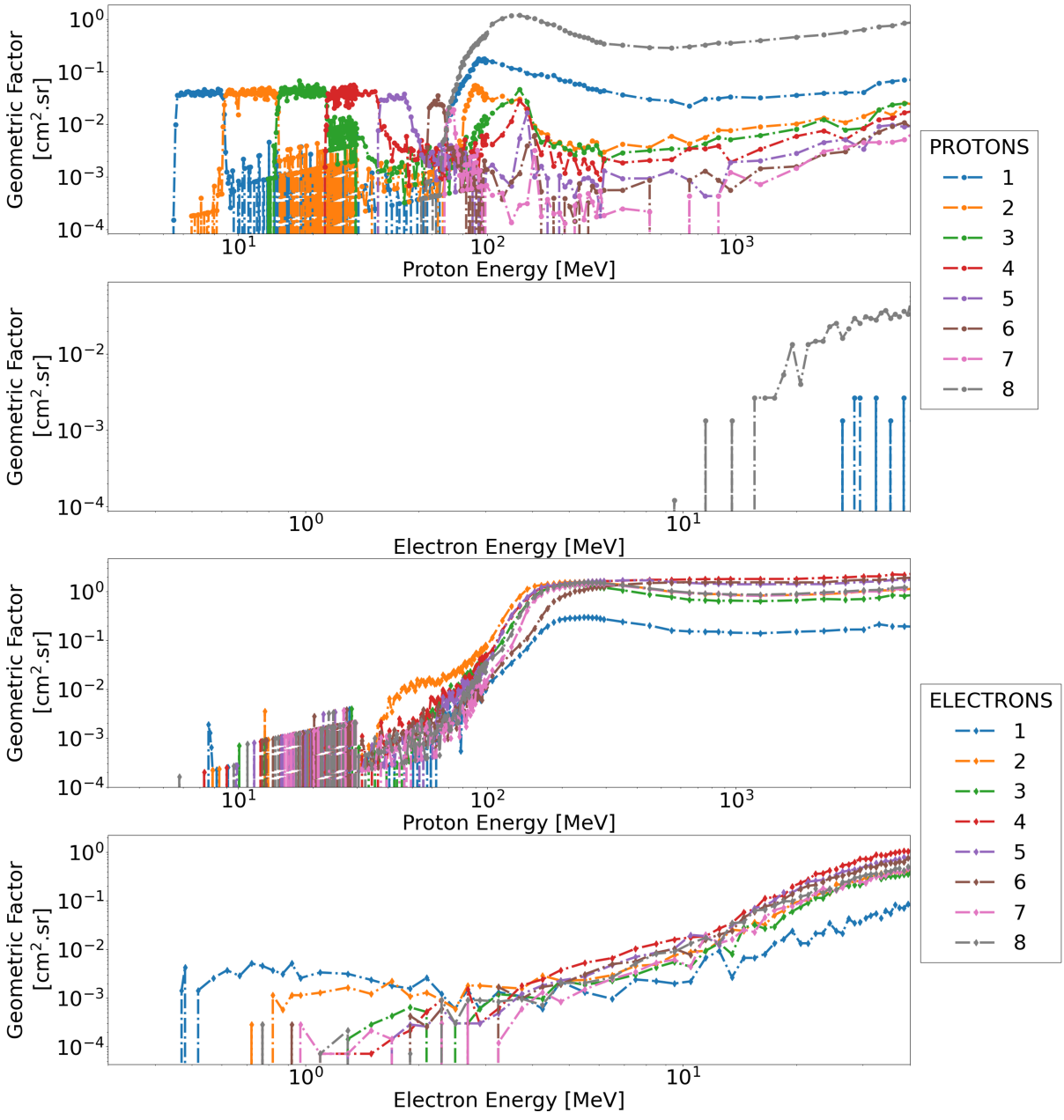

Figure 1. RADEM response functions. The top two panels show the sensitivity of the PROTONS detection bins to protons and electrons, respectively. The bottom two panels show the sensitivity of the ELECTRONS detection bins to protons and electrons. Adapted from Pinto et al. (2026)

https://doi.org/10.5194/egusphere-2026-2055
Preprint. Discussion started: 15 April 2026

Table 1. Energy sensitivity of each PROTONS and ELECTRONS detection bin.

Variable	Entry	Detector	Electron Energy Interval (MeV)	Proton Energy Interval (MeV)
PROTONS	1	PDH	>20.0	5.70-8.90 & >70.0
	2		Not sensitive	8.90-14.2 & 80.0-173
	3		Not sensitive	14.7-22.7
	4		Not sensitive	22.7-31.5
	5		Not sensitive	37.5-45.0
	6		Not sensitive	58.0-70.0
	7		Not sensitive	70.0-78.0
	8		>10.0	>56.0
ELECTRONS	1	EDH	>0.47	7.65-7.95 & >45.0
	2		>0.88	>45.0
	3		>1.70	>45.0
	4		>2.00	>55.0
	5		>2.00	>65.0
	6		>2.00	>70.0
	7		>2.00	>70.0
	8		>2.00	>70.0

3 Lunar-Earth Gravity Assist

Between August 19 and 20, 2024, the JUICE spacecraft executed the first ever dual gravity-assist manoeuvre using both the Moon and Earth (Dietz et al., 2026). This was the mission's first gravity assist and redirected the spacecraft toward the inner Solar System, placing it on a trajectory to encounter Venus, a gravity assist that occurred in August 2025. JUICE approached the Earth–Moon system from the night side. First, it flew past the Moon on August 19, with closest approach (C.A.) occurring at 21:16 UT at an altitude of 752 km. The Earth gravity assist took place on the following day, with C.A. at 21:56 UT at an altitude of 6839 km. The LEGA provided a unique test environment for the JUICE instruments including RADEM. A detailed timeline of the LEGA sequence is shown in Figure 2.

3.1 Earth Inner Magnetosphere

During the Earth gravity assist, JUICE traversed the magnetotail before moving inward to the inner magnetosphere. The near-Earth magnetosphere, spanning approximately 1 to $10\,\mathrm{R_E}$, is dominated by Earth's intrinsic dipole magnetic field and is commonly referred to as the inner magnetosphere (Kanekal and Miyoshi, 2021). Its structure varies with particle energy and can be divided into three main, overlapping regions: (1) the plasmasphere (Goldstein, 2006), consisting of low-energy ionospheric plasma driven by co-rotational and convection electric fields; (2) the ring current (Ebihara and Ejiri, 2003), formed by medium-energy electrons and ions drifting in opposite directions due to magnetic field gradients and curvature; and (3)

https://doi.org/10.5194/egusphere-2026-2055
Preprint. Discussion started: 15 April 2026

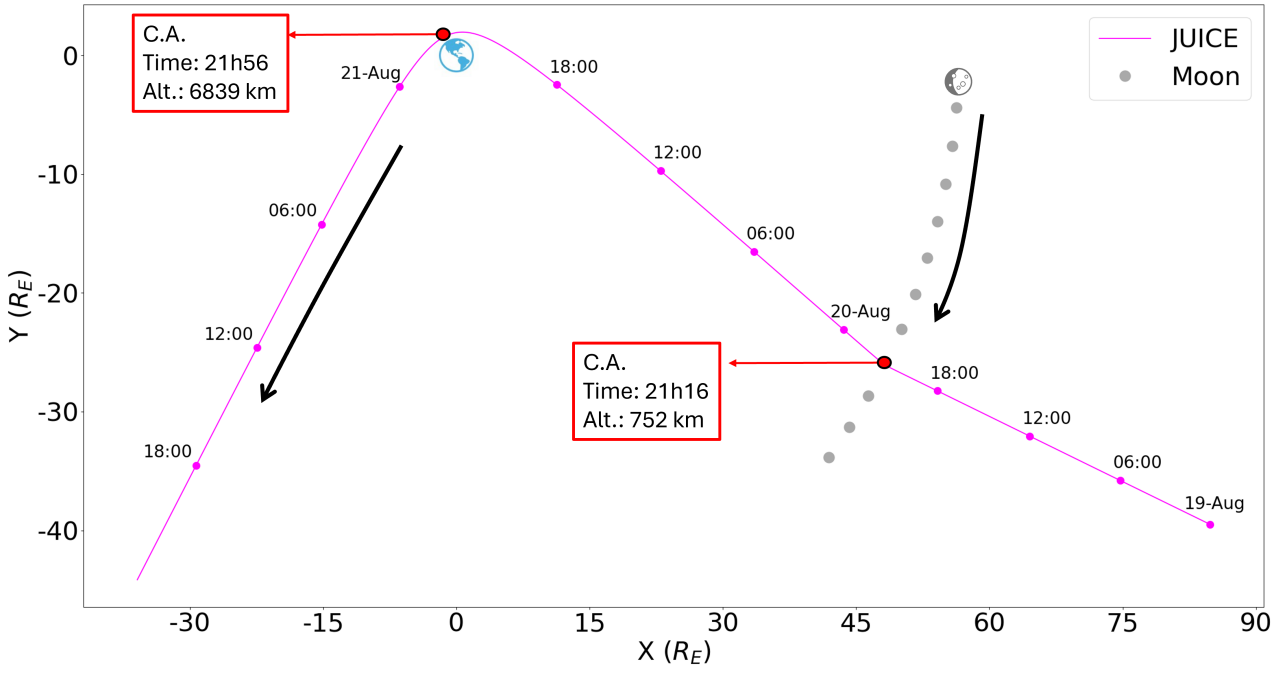

Figure 2. LEGA projection on the Earth mean ecliptic J2000 plane. On August 19, 2024, JUICE flew by the Moon with a C.A. of about 750 km altitude at 21h16 UTC. On the following day, it passed by Earth going down to an altitude of about 6840 km at 21h56 UTC.

the Van Allen radiation belts (Kanekal and Miyoshi, 2021), populated by trapped high-energy charged particles (primarily electrons and protons).

The radiation belts extend from a few hundred kilometers above the Earth's surface out to $L \approx 10$, where the L-shell parameter approximates the magnetic equatorial radial distance of a magnetic field line in units of $\mathrm{R_E}$. The belts are traditionally divided into two distinct zones. The outer belt ($L \approx 3$–10) is highly variable and typically dominated by electrons originating from the solar wind, with energies ranging from tens of keV to several MeV.

Closer to Earth, the inner belt ($L \approx 1.2$–2.5) is remarkably stable and dominated by protons with energies that can exceed 100 MeV. This inner-belt population is primarily generated through the decay of albedo neutrons produced by cosmic rays interacting with Earth's atmosphere (Selesnick et al., 2014), as well as contributions from SEP events. In addition to this proton population, a substantial flux of sub-relativistic electrons is also present in this region. Separating the inner and the outer electron radiation belts is the so-called slot region, where electron fluxes are diminished on average, due to rapid pitch angle scattering electron losses by waves (Li et al., 2023).

3.2 Observations of the Van Allen Belts

Figure 3 summarizes RADEM (first panel) measurements during the JUICE Earth flyby. In the second panel, JMAG (Amtmann et al., 2024) low-cadence (60-second) measurements are compared to the CHAOS-7 model (Finlay et al., 2020), showing

https://doi.org/10.5194/egusphere-2026-2055
Preprint. Discussion started: 15 April 2026

excellent agreement. A more detailed analysis of JMAG LEGA observations can be found in LaMoury et al. (2026). Panels 3-5 show the pitch angle of the RADEM FOV calculated with the magnetic field vector from JMAG, the L-shell computed assuming a dipole field and the magnetic local time (MLT), respectively. A more precise determination of the L-shell for non-dipolar fields is not critical for the data presented in this manuscript. Panel 6 shows the JUICE altitude in relation to the Earth's surface.

In the inbound leg of the flyby, the ELECTRONS detection bins' count rates began increasing around 19:13 UT and reached a maximum at 21:02 UT, corresponding to the spacecraft crossing the outer radiation belt. A secondary peak at 20:29 UT is visible in the lower-energy electron bins, indicating finer structure within the outer belt.

The PROTONS detection bins' count rates started rising at 21:10 UT and peaked at 21:49 UT, consistent with the inner belt. A secondary maximum was observed at 21:28 UT and a plateau was found between 22:14 UT and 22:28 UT. Notice that the peak PROTONS count rate occurred seven minutes before C.A. A possible reason for this offset is that the trapped inner-belt pitch-angle distribution is anisotropic, strongly peaking at 90° (perpendicular to the local magnetic field). As shown in the third panel of Fig. 3, the PDH FOV was centered near a 90° pitch angle at the time of the peak count rate. By the time of C.A., the instrument's FOV had shifted away by approximately 5°. However, even though the PDH has a narrow aperture (20°), this small deviation from 90° is not sufficient to justify such a difference in the total flux. Also, since the C.A. was above the Pacific Ocean, the asymmetry observed is not due to a crossing of the South Atlantic Anomaly. A more likely reason is that, due to the geometry of the flyby, C.A. in radial distance did not coincide with minimum magnetic latitude. The peak count rate therefore occurred when JUICE was closer to the magnetic equator, where the trapped inner-belt proton flux is expected to be higher.

The ELECTRONS 1 detection bin also had a peak inside the slot region at 21:39 UT. This detection bin measures electrons above approximately 450 keV. While the detection bin can also respond to protons, its spatial profile is clearly different from that of the PROTONS detection bins. The other ELECTRONS detection bins' count rates were close to their background levels during this period, which is in line with the crossing of the slot region and partly into the inner radiation belt, which is devoid of >1 MeV electrons. Their count rates started increasing again at 22:17 UT, peaking at 22:45 UT and then again at 23:29 UT, which corresponds to the outbound pass through the outer belt. All detection bins returned to background levels at 00:35 UT marking the spacecraft's exit from the outer electron radiation belt.

Most importantly, the time profiles of the ELECTRONS- and PROTONS-bins, even at regions of the most intense proton radiation, seem uncorrelated. This means that the ELECTRONS channel logic effectively rejects spurious signals from low- to mid-energy protons, which has been a source of misleading measurements in the inner electron belt, for decades attributed to ultra-relativistic electrons and until the Van Allen probes mission (Claudepierre et al., 2019).

3.3 Electrons

Even though the RADEM electron detection bins are integrated in energy (see Fig. 1), we estimated the differential fluxes using the bow-tie method assuming a maximum electron energy of 7 MeV (Boudouridis et al., 2020; Pinto et al., 2026). Fig. 4 shows these differential electron fluxes as a function of dipole L-shell (top panel), together with the total magnetic field and MLT (bottom panel).

https://doi.org/10.5194/egusphere-2026-2055
Preprint. Discussion started: 15 April 2026

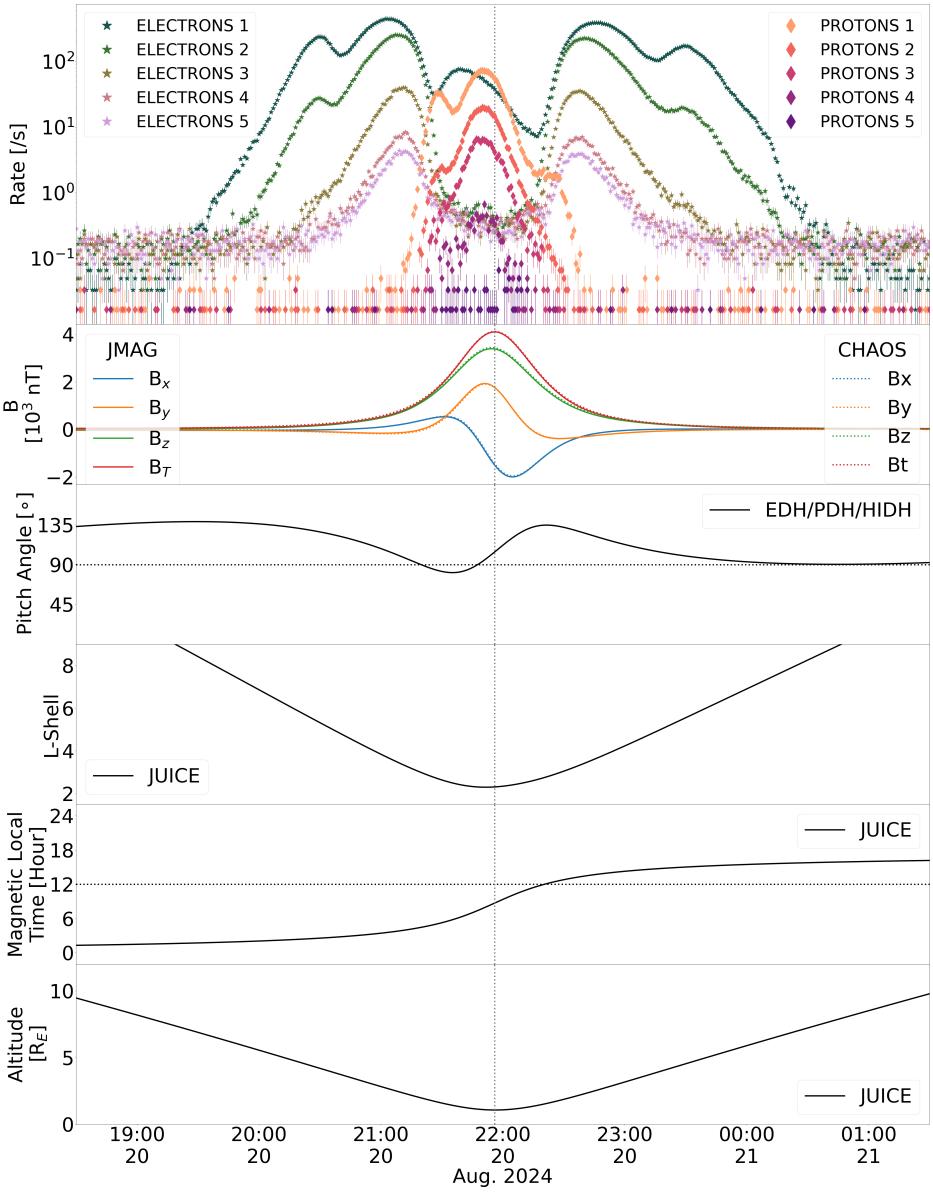

Figure 3. Summary of the RADEM observations during the Earth flyby. The top panel shows count rates of selected RADEM PROTONS (diamonds) and ELECTRONS (stars) detection bins. Each color corresponds to an individual detection bin. Their energy sensitivity is given in Table 1. The second panel presents the B_X (blue), B_Y (orange), B_Z (green), and B_T (red) magnetic field measured by JMAG (solid lines) and estimated with the CHAOS model (dashed lines). The third panel shows the EDH, PDH, and HIDH pitch angles calculated from the JMAG magnetic field measurements. The fourth and fifth panels show trajectory parameters derived from the CHAOS model, including L-shell and MLT. The bottom panel shows the spacecraft altitude. C.A. occurred at 21:56 UT at an altitude of 6840 km.

https://doi.org/10.5194/egusphere-2026-2055
Preprint. Discussion started: 15 April 2026

The inbound and outbound electron flux profiles are generally similar, but display clear differences in the apparent L-shell of the outer peak ($L > 5.5$). The depth of the flux minimum between the inner and outer belts (slot region) was also much lower during the outbound pass than during the inbound pass. The apparent spatial differences between the inbound and outbound flux profiles at high L-shells are likely due to mapping the complex magnetospheric geometry to a simple dipole L-shell and/or to magnetospheric dynamics. The simple dipole does not capture effects of MLT asymmetries: JUICE approached the Earth through the stretched night/dawn sector (MLT $\approx$ 0–6) and departed through the relatively compressed afternoon/dusk sector (MLT $\approx$ 16–18). This typically has the opposite effect on the electron drift shells, with electron drifts approaching closer to the planet at midnight, while stretching out at the dayside (Elkington et al., 1999). Consequently, for a given dipole L-shell in the outer belt (L>4.5), the inbound and outbound legs sampled different local magnetic field strengths (B_t), resulting in the observed asymmetry of the measured electron flux.

On the other hand, the inbound/outbound differences seen within the slot region and for the electron bins <0.72 MeV, are too strong to be attributed to magnetospheric field asymmetries. These are likely caused by dynamical processes, specifically by sudden particle enhancements at low L-shells (SPELLS), <1 MeV transients known to fill the slot region and supply the inner radiation belt with <1 MeV electron flux (Turner et al., 2017). SPELLS decay over timescales of days, meaning that the observed inbound/outbound asymmetry may not simply reflect their time evolution, but rather indicates that their occurrence is not uniform and is instead constrained in longitude

The dual peak observed in both the inbound and outbound portions of the flyby is commonly seen at relativistic energies (> 1 MeV) following strong geomagnetic storms. In JUICE/RADEM, these peaks are primarily observed in the two lowest ELECTRONS detection bins (ELECTRONS 1 and ELECTRONS 2). During the flyby, geomagnetic conditions were relatively quiet (Dst ≈ -10 nT). However, as shown in the bottom panel of Figure 5, on August 12, eight days earlier, an intense geomagnetic storm (Dst ≈ -185 nT) impacted Earth and significantly disturbed the radiation belts.

As shown in Fig. 5, the proton (top panel) and electron (middle panel) fluxes measured by the GOES-18 Solar and Galactic Proton Sensors (SGPS, Kress et al., 2021) and the Magnetospheric Electrons and Protons: Medium and High Energy (MPSH, Kress et al., 2020; Dichter et al., 2015) instruments were strongly affected by the 12 August storm. A secondary, weaker storm occurred on 17 August and further disturbed the outer belt.

As described by Yuan and Zong (2013) and Kress et al. (2014), such storms typically produce a rapid dropout of outer-belt electrons during the main phase. The belts subsequently rebuild during the recovery phase, and after about 1–2 days the electron distribution can evolve into two distinct L-shell peaks, with an inner peak forming first and an outer peak developing later. This configuration can persist for days or even weeks, so the dual-peak structure observed by RADEM is consistent with a genuine feature of the electron population sampled during the flyby.

Ultimately, these measurements show that RADEM can measure energetic electrons, successfully achieving its main LEGA objective.

https://doi.org/10.5194/egusphere-2026-2055
Preprint. Discussion started: 15 April 2026

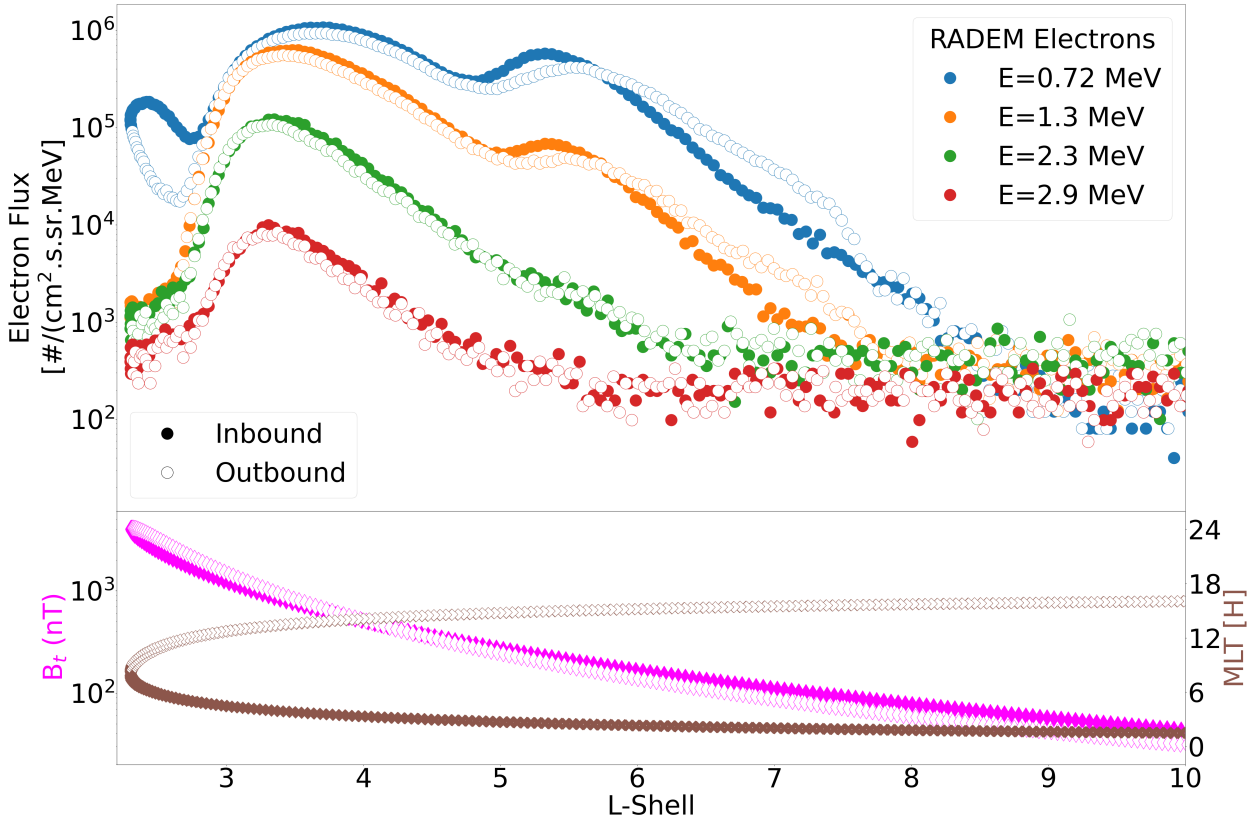

Figure 4. Electron flux of trapped electrons as a function of dipole L-shell (top panel). The flux is derived from RADEM measurements using the bow-tie analysis method (Boudouridis et al., 2020; Pinto et al., 2026). Each color corresponds to a different effective energy. The inbound and outbound segments of the trajectory are distinguished by solid and open markers, respectively, across all energy channels. The bottom panel illustrates the local magnetic field magnitude (B_t, magenta, left axis) and the spacecraft's MLT (brown, right axis), highlighting the day-night magnetospheric asymmetry that drives the asymmetry of the flux profiles at higher L-shells.

3.4 Protons

Figure 6 shows the trapped proton flux measured by RADEM as a function of dipole L-shell for multiple proton energies. The proton flux was derived using the bow-tie analysis method as described in Pinto et al. (2026). All energy channels exhibit a pronounced maximum near $L \approx 2.2$, corresponding to the core of the inner radiation belt. Beyond this peak, the flux decreases rapidly with increasing L-shell, indicating a strong outward radial gradient characteristic of trapped high-energy proton populations.

The inbound flux is about an order of magnitude higher than the outbound flux. Unlike the outer-belt electrons, this asymmetry at low L-shells ($L < 4$) is too strong to simply arise from the non-dipolar shape of the magnetosphere. Contributions may come from the JUICE magnetic latitude, that influences the equatorial pitch angle of the observed protons: trapped radiation

https://doi.org/10.5194/egusphere-2026-2055
Preprint. Discussion started: 15 April 2026

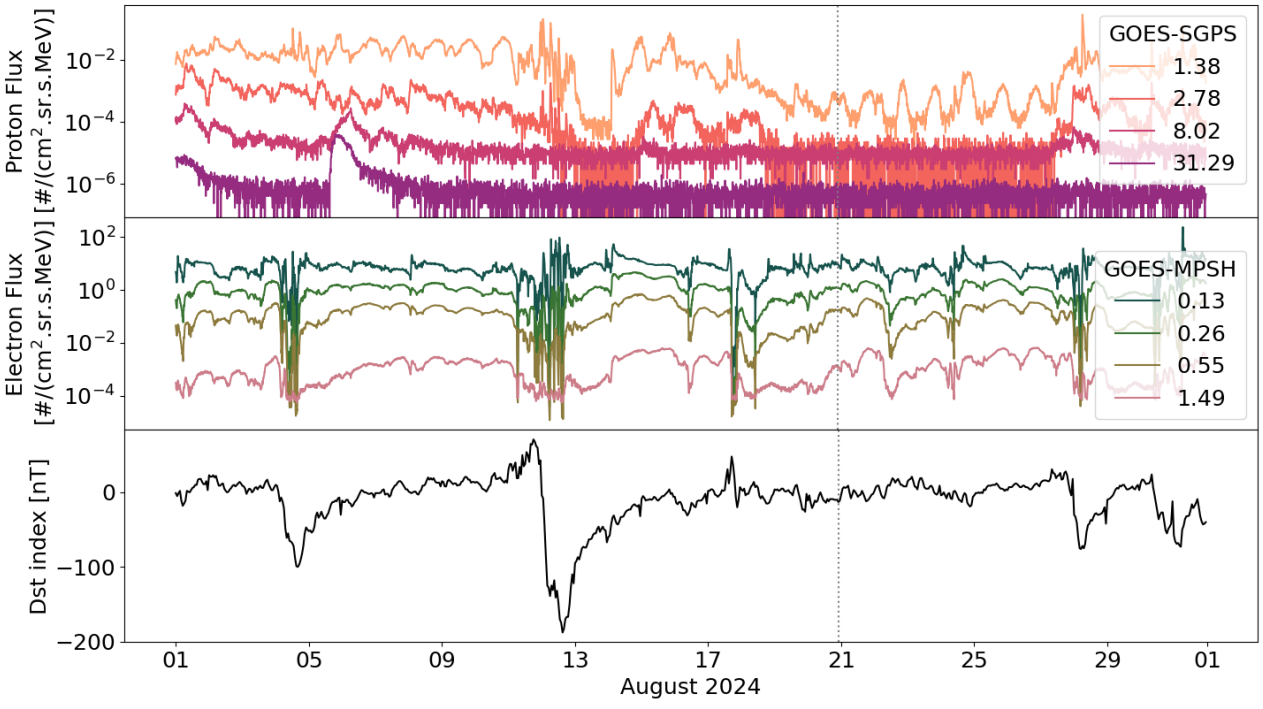

Figure 5. Geomagnetic and energetic particle environment during the August 2024 JUICE flyby. (Top) Proton flux measurements from the GOES-18 SGPS instrument. (Middle) Electron flux measurements from the GOES-18 MPSH instrument. Different colors represent different energies in both electron and proton fluxes. (Bottom) Dst index (black line) provided by the World Data Center for Geomagnetism, Kyoto, indicating geomagnetic conditions. The vertical dashed line marks the C.A. of the JUICE Earth flyby.

belt protons have strongly anisotropic pitch-angle distributions, with the highest fluxes expected for equatorially mirroring particles (Selesnick and Albert, 2019). During the inbound leg, JUICE crossed the inner belt closer to the magnetic equator, where the local magnetic field B_t is weaker. During the outbound pass at the same L-shell, the spacecraft was at higher magnetic latitude and higher B_t, resulting in a lower measured flux. This explanation may apply for smaller scale inbound/outbound asymmetries seen at L<2.6.

A secondary enhancement is visible centered on the inbound leg near $L \approx 2.8$, particularly in the lower-energy channels. The inbound/outbound flux difference there, especially for 7.4 and 11.1 MeV protons at 2.6<L<3.0, is too large to be solely attributed to geometrical effects. This feature is collocated with the inner edge of the ring current. A transient solar proton component is likely to lead to local time/longitudinal asymmetries in the MeV proton distribution at such distances(Selesnick and Albert, 2019). At higher L-shells, the flux goes back to the instrument background, showing an energy-dependent outer boundary.

https://doi.org/10.5194/egusphere-2026-2055
Preprint. Discussion started: 15 April 2026

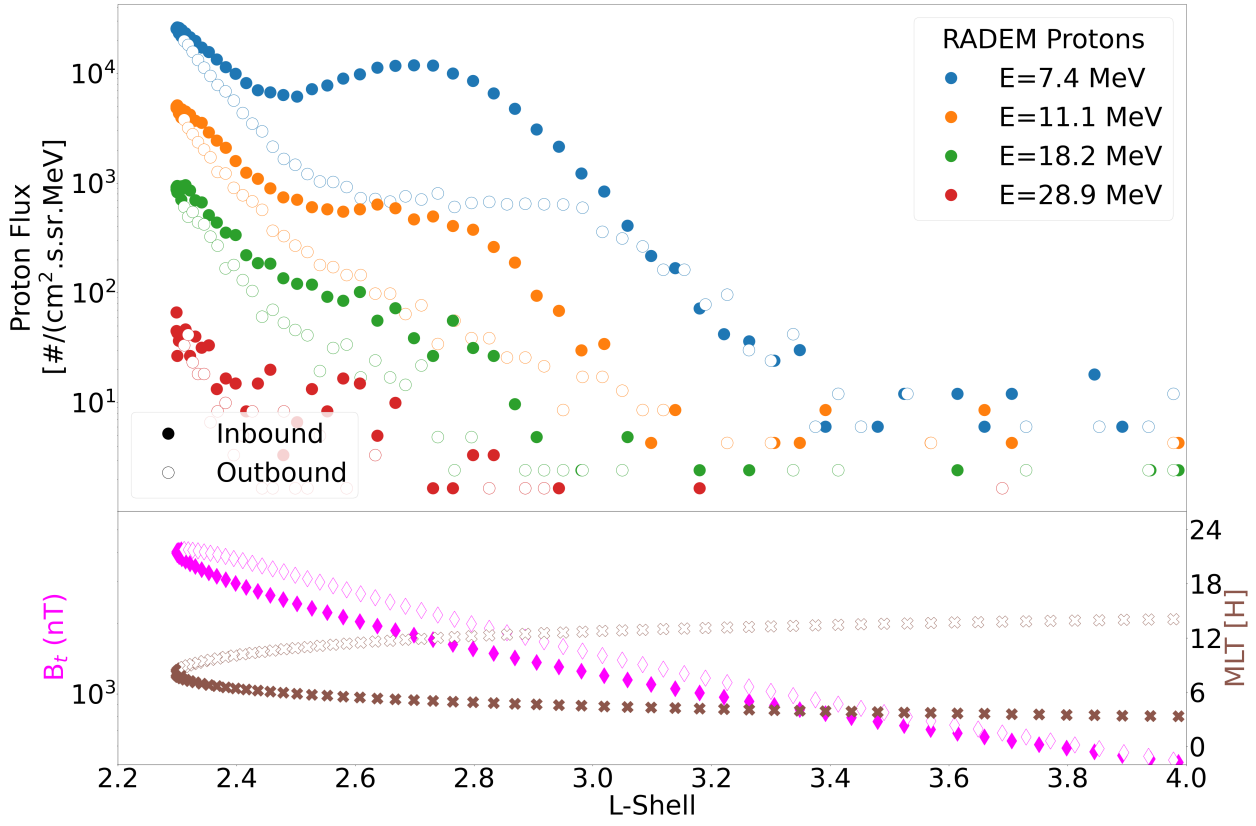

Figure 6. Flux of trapped protons as a function of dipole L-shell (top panel). The flux is derived from RADEM measurements using the bow-tie analysis method described in Pinto et al. (2026). Each color corresponds to a different effective energy. The inbound and outbound segments of the trajectory are distinguished by solid and open markers, respectively, across all energy channels. The bottom panel illustrates the local magnetic field magnitude (B_t, magenta, left axis) and the spacecraft MLT (brown, right axis), highlighting the difference in magnetic field strength along the trajectory, which is consistent with the inbound/outbound asymmetry in the inner-belt proton flux profiles.

3.5 Moon Flyby

During LEGA, JUICE flew past the Moon at an altitude of about 750 km, in the Earth's magnetotail lobes and well outside the main trapped-particle regions of Earth's magnetosphere. In this interval, RADEM was therefore expected to measure mainly its interplanetary background of GCRs (Liuzzo et al., 2024). At this altitude, the main effect that was expected was a small decrease in count rate caused by occultation of part of the sky by the lunar disk.

Figure 7 compares the predicted lunar shadowing fraction with the combined normalized count rate from the RADEM detectors. A slight decrease is visible near C.A., but it is much smaller than the geometric prediction, which does not account for the angular response of the individual detector heads. The instrument time resolution is also too slow to capture the sharp

https://doi.org/10.5194/egusphere-2026-2055
Preprint. Discussion started: 15 April 2026

temporal gradient of the predicted shadowing fraction. Given the low count rate during the flyby and the detector viewing geometry, this effect cannot be quantified reliably, and we therefore consider the result inconclusive.

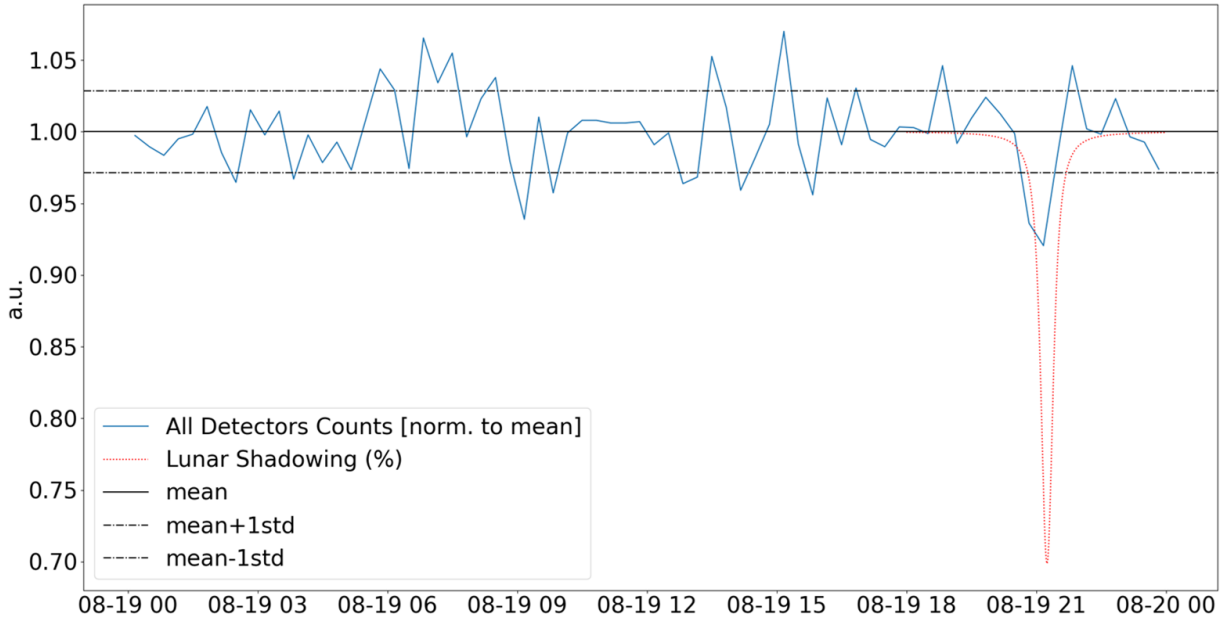

Figure 7. Normalized count rate from all RADEM detectors as a function of time during the lunar flyby on 19 August 2024. The blue curve shows the total detector count rate normalized to its mean value. The solid black line indicates the mean count rate, and the dash-dotted lines represent ±1 standard deviation. The red dotted curve shows the predicted geometric lunar shadowing fraction.

4 Conclusions and Future Operations

The Jupiter Icy Moons Explorer (JUICE) successfully completed the first-ever Lunar–Earth Gravity Assist (LEGA) in August 2024. This manoeuvre provided the first opportunity to evaluate the performance of the RADiation-hard Electron Monitor in a trapped planetary-radiation environment. The instrument's primary objective during LEGA—to demonstrate its ability to detect trapped electrons—was achieved.

In the outer electron radiation belt, RADEM observed a dual-peak electron structure that is consistent with the recovery phase of an intense geomagnetic storm that occurred days before the flyby. RADEM also captured large-scale asymmetries in both the inner and the outer magnetosphere, with the difference between the inbound and outbound electron fluxes reflecting the day–night distortion of the local magnetic field, pitch angle coverage effects and dynamics, either associated to sudden particle enhancements at low L shells (SPELLS) in the slot region, or to transient ring current proton populations further out, possibly remnants of solar energetic particle entry. In the inner magnetosphere, RADEM further mapped the highest-energy

https://doi.org/10.5194/egusphere-2026-2055
Preprint. Discussion started: 15 April 2026

proton population with a pronounced flux maximum near $L \approx 2.2$ where JUICE had its closest approach. At that distance and for proton energies below 45 MeV shown here, the proton spectrum mixes contributions from solar energetic particles and from galactic cosmic ray secondaries. The latter results in a process known as Cosmic Ray Albedo Neutron Decay (CRAND) (Selesnick et al., 2014).

Finally, the close lunar flyby was accompanied by at most a small decrease in the total RADEM count rate near C.A. However, this effect remained inconclusive because the expected signature was weak, the count rate was low, and the detector viewing geometry reduced the observable shadowing relative to the geometric estimate.

Together, these LEGA observations validate RADEM's capability to measure electrons and strengthen the characterization of its proton detection bins. The separation of these two species, especially at the most intense radiation belt region where the most penetrating proton and electron spectra are mixed, validates the coincidence logic of RADEM. This flyby therefore provides an important in-flight validation data set ahead of the mission's science phase at Jupiter.

In the future, the calibration campaign reported in Pinto et al. (2026) will be repeated and the sensitivity of the electron detection bins will be improved. We also expect to reduce contamination of the electron channels by high-energy protons by adding coincidences between EDH sensors to the coincidence logic. The second and third JUICE Earth gravity assists will be used to validate these changes and to prepare for operations at Jupiter.

Data availability. RADEM data are not subject to a proprietary period and is publicly available through ESA Planetary Science Archive. The JMAG data acquired during the JUICE Moon–Earth gravity assist in August 2024 are currently under the mission's cruise-phase proprietary period. These data will be made available through the ESA Planetary Science Archive following the first Cruise Archive Delivery, which is currently scheduled for six months after the third Earth Gravity Assist in 2029.

Author contributions. Marco Pinto performed the data analysis and prepared the manuscript. André Rodrigues and Luísa Arruda assembled the RADEM electron data. Elias Roussos, Daniel Schmid, Martin Volwerk and Stavros Kotsiaros contributed to the interpretation of the radiation belt observations. Patrick Brown and Michele Dougherty provided the JMAG data and contributed to its interpretation. All authors contributed to the successful implementation of the manuscript.

Competing interests. At least one of the (co-)authors is a member of the editorial board of Annales Geophysicae.

Acknowledgements. The work of M. Pinto, A. Rodrigues, and L. Arruda was performed under an ESA contract: 4000137865/22/ES/JD Expert Support to BERM & RADEM units. Imperial College authors are supported by the UK Space Agency award ST/X002357/1.

https://doi.org/10.5194/egusphere-2026-2055
Preprint. Discussion started: 15 April 2026

References

Amtmann, C., Pollinger, A., Ellmeier, M., Dougherty, M., Brown, P., Lammegger, R., Betzler, A., Agú, M., Hagen, C., Jernej, I., Wilfinger, J., Baughen, R., Strickland, A., and Magnes, W.: Accuracy of the scalar magnetometer aboard ESA's JUICE mission, Geoscientific Instrumentation, Methods and Data Systems, 13, 177–191, https://doi.org/10.5194/gi-13-177-2024, 2024.

Barabash, S., Brandt, P. C., Wurz, P., and the PEP Team: Particle Environment Package (PEP) for the ESA JUICE Mission, in: 3rd International Workshop on Instrumentation for Planetary Missions, 2016.

Bolton, S. J. et al.: Ultra-relativistic electrons in Jupiter's radiation belts, Nature, 415, 987–991, https://doi.org/10.1038/415987a, 2002.

Bolton, S. J. et al.: The JUNO Mission, Space Science Reviews, 213, 5–37, 2017.

Boudouridis, A., Rodriguez, J. V., Kress, B. T., Dichter, B. K., and Onsager, T. G.: Development of a bowtie inversion technique for real-time processing of the GOES-16/-17 SEISS MPS-HI electron channels, Space Weather, 18, e2019SW002 403, https://doi.org/10.1029/2019SW002403, 2020.

Boutonnet, J. et al.: The JUICE Spacecraft System Design, Space Science Reviews, 222, 35, https://doi.org/10.1007/s11214-026-01289-4, 2026.

Clark, G., Kollmann, P., Kinnison, J., Kelly, D., Haapala, A., Li, W., Jaynes, A. N., Blum, L., Marshall, R., Turner, D., Cohen, I., Ukhorskiy, A., Mauk, B. H., Roussos, E., Nénon, Q., Drozdov, A., Woodfield, E., Dunn, W., Berland, G., Kraft, R., Williams, P. K. G., Smith, H. T., Hospodarsky, G., Wu, X., Hulsman, J., O'Brien, T. P., Looper, M., Sorathia, K., Sciola, A., Sicard, A., Donegan, M., Clare, B., Emmell, D., Wirzburger, J., Sepulveda, D., Roufberg, L., Perry, J., Schellhase, J., Pergosky, D., Able, E., O'Neill, M., Fernandes, C., Chattopadhyay, D., Bibelhauser, S., Kijewski, S., Pulkowski, J., Furrow, M., Feldman, C., Nichols, J., Carr, N., Verma, H., Lindsay, S., Bunce, E., Parry, B., and Martindale, A.: Comprehensive Observations of Magnetospheric Particle Acceleration, Sources, and Sinks (COMPASS): A Mission Concept to Explore the Extremes of Jupiter's Magnetosphere, , 222, 15, https://doi.org/10.1007/s11214-025-01249-4, 2026.

Claudepierre, S. G., O'Brien, T. P., Looper, M. D., Blake, J. B., Fennell, J. F., Roeder, J. L., Clemmons, J. H., Mazur, J. E., Turner, D. L., Reeves, G. D., and Spence, H. E.: A Revised Look at Relativistic Electrons in the Earth's Inner Radiation Zone and Slot Region, Journal of Geophysical Research (Space Physics), 124, 934–951, https://doi.org/10.1029/2018JA026349, 2019.

Denk, T., Williams, D. A., Tosi, F., Bell, III, J. F., Mottola, S., de Pater, I., Lainey, V., Molyneux, P., Matz, K.-D., Hartogh, P., et al.: Io and the Minor Jovian Moons – Prospects for JUICE, Space Science Reviews, 222, 27, https://doi.org/10.1007/s11214-025-01263-6, 2026.

Dichter, B. K., Galica, G. E., McGarity, J. O., Tsui, S., Golightly, M. J., Lopate, C., and Connell, J. J.: Specification, design and calibration of the space weather suite of instruments on the NOAA GOES-R program spacecraft, IEEE Transactions on Nuclear Science, 62, 2776–2783, https://doi.org/10.1109/TNS.2015.2477997, 2015.

Dietz, A., Boutonnet, A., and Budnik, F.: The JUICE Lunar-Earth gravity assist from trajectory design, navigation and spacecraft operations perspective, EGUsphere, 2026, 1–17, https://doi.org/10.5194/egusphere-2026-1015, 2026.

Dodd, P. E. and Massengill, L. W.: Basic mechanisms and modeling of single-event upset in digital microelectronics, IEEE Trans. Nucl. Sci., 50, 583–602, https://doi.org/10.1109/TNS.2003.813129, 2003.

Ebihara, Y. and Ejiri, M.: Numerical Simulation of the Ring Current: Review, Space Science Reviews, 105, 377–452, https://doi.org/10.1023/A:1023905607888, 2003.

Elkington, S. R., Hudson, M. K., and Chan, A. A.: Acceleration of relativistic electrons via drift-resonant interaction with toroidal-mode Pc-5 ULF oscillations, , 26, 3273–3276, https://doi.org/10.1029/1999GL003659, 1999.

https://doi.org/10.5194/egusphere-2026-2055
Preprint. Discussion started: 15 April 2026

Finlay, C. C., Kloss, C., Olsen, N., Hammer, M. D., Tøffner-Clausen, L., Grayver, A., and Kuvshinov, A.: The CHAOS-7 geomagnetic field model and observed changes in the South Atlantic Anomaly, Earth, Planets and Space, 72, 156, https://doi.org/10.1186/s40623-020-01252-9, 2020.

Fletcher, L. N., Cavalié, T., Grassi, D., et al.: Jupiter Science Enabled by ESA's Jupiter Icy Moons Explorer, Space Science Reviews, 219, 2023.

Goldstein, J.: Plasmasphere Response: Tutorial and Review of Recent Imaging Results, Space Science Reviews, 124, 203–216, https://doi.org/10.1007/s11214-006-9105-y, 2006.

Grasset, O. et al.: JUpiter ICy moons Explorer (JUICE): An ESA mission to orbit Ganymede and to characterize the Jupiter system, Planet. Space Sci., 78, 1–21, 2013.

Hajdas, W., Gonçalves, P., Pinto, M., et al.: The JUICE Radiation Environment Monitor, RADEM, Space Science Reviews, 221, 2025.

Kanekal, S. and Miyoshi, Y.: Dynamics of the terrestrial radiation belts: a review of recent results during the VarSITI (Variability of the Sun and Its Terrestrial Impact) era, 2014–2018, Progress in Earth and Planetary Science, 8, 35, https://doi.org/10.1186/s40645-021-00413-y, 2021.

Kollmann, P., Roussos, E., Paranicas, C., Woodfield, E. E., Mauk, B. H., Clark, G., et al.: Electron acceleration to MeV energies at Jupiter and Saturn, Journal of Geophysical Research: Space Physics, 123, 9110–9129, https://doi.org/10.1029/2018JA025665, 2018.

Kress, B. T., Hudson, M. K., and Paral, J.: Rebuilding of the Earth's outer electron belt during 8–10 October 2012, Geophysical Research Letters, 41, 749–754, https://doi.org/10.1002/2013GL058588, 2014.

Kress, B. T., Rodriguez, J. V., and Onsager, T. G.: The GOES-R Space Environment In Situ Suite (SEISS): Measurement of energetic particles in geospace, in: The GOES-R Series, edited by Steven, J. G., Schmit, T. J., Daniels, J., and Redmon, R. J., pp. 243–250, Elsevier, https://doi.org/10.1016/B978-0-12-814327-8.00020-2, 2020.

Kress, B. T., Rodriguez, J. V., Boudouridis, A., Onsager, T. G., Dichter, B. K., Galica, G. E., and Tsui, S.: Observations from NOAA's newest solar proton sensor, Space Weather, 19, e2021SW002 750, https://doi.org/10.1029/2021SW002750, 2021.

LaMoury, A.T., S. L. B. B. et al.: First results from the JUICE magnetometer during the Lunar Earth Gravity Assist, EGUsphere, 2026, 2026.

Lario, D., Wijsen, N., Kwon, R. Y., Sánchez-Cano, B., Richardson, I. G., Pacheco, D., Palmerio, E., Stevens, M. L., Szabo, A., Heyner, D., Dresing, N., Gómez-Herrero, R., Carcaboso, F., Aran, A., Afanasiev, A., Vainio, R., Riihonen, E., Poedts, S., Brüden, M., Xu, Z. G., and Kollhoff, A.: Influence of Large-scale Interplanetary Structures on the Propagation of Solar Energetic Particles: The Multispacecraft Event on 2021 October 9, The Astrophysical Journal, 934, 55, https://doi.org/10.3847/1538-4357/ac6efd, 2022.

Li, Y. X., Yue, C., Liu, Y., Zong, Q.-G., Zou, H., and Ye, Y. G.: Dynamics of the inner electron radiation belt: A review, Earth and Planetary Physics, 7, 109–118, https://doi.org/10.26464/epp2023009, 2023.

Liuzzo, L., Poppe, A. R., Lee, C. O., and Angelopoulos, V.: Solar Energetic Electron Access to the Moon Within the Terrestrial Magnetotail and Shadowing by the Lunar Surface, , 51, e2024GL110228, https://doi.org/10.1029/2024GL110228, 2024.

Masters, A., Modolo, R., Roussos, E., et al.: Magnetosphere and Plasma Science with the Jupiter Icy Moons Explorer, Space Science Reviews, 221, 2025.

Nénon, Q., Miller, L. P., Kollmann, P., et al.: Pitch Angle Distribution of MeV Electrons in the Magnetosphere of Jupiter, Journal of Geophysical Research, 127, e30 627, https://doi.org/10.1029/2022JA030627, 2022.

Oldham, T. R. and McLean, F. B.: Total ionizing dose effects in MOS oxides and devices, IEEE Trans. Nucl. Sci., 50, 483–499, https://doi.org/10.1109/TNS.2003.812927, 2003.

https://doi.org/10.5194/egusphere-2026-2055
Preprint. Discussion started: 15 April 2026

Pinto, M., Gonçalves, P., Marques, A., Costa Pinto, J., and Hajdas, W.: Development of a Directionality Detector for RADEM, the Radiation Hard Electron Monitor aboard the JUICE Mission, IEEE Trans. Nucl. Sci., 66, 1770–1777, https://doi.org/10.1109/TNS.2019.2900398, 2019.

Pinto, M., Santos, F., Gomes, A., Gonçalves, T. M., Arruda, L., Gonçalves, P., Rodríguez-García, L., Vainio, R., Witasse, O., and Altobelli, N.: In-flight calibration of RADEM, the JUICE mission radiation monitor, Astronomy Astrophysics, https://doi.org/10.1051/0004-6361/202558601, accepted; forthcoming, 2026.

Pinto, M. G. A.: Development of a Directionality Detector and Radiation Hardness Assurance for RADEM, the ESA JUICE Mission Radiation Monitor, Ph.D. thesis, Instituto Superior Técnico (Universidade de Lisboa), 2019.

Potgieter, M. S.: Solar Modulation of Cosmic Rays, Living Rev. Sol. Phys., 10, 3, https://doi.org/10.12942/lrsp-2013-3, 2013.

Reames, D. V.: The Two Sources of Solar Energetic Particles, Space Science Reviews, 175, 53–92, https://doi.org/10.1007/s11214-013-9958-9, 2013.

Rodríguez-García, L., Palmerio, E., Pinto, M., Dresing, N., Cohen, C. M. S., Gómez-Herrero, R., Gieseler, J., Santos, F., Espinosa Lara, F., Cernuda, I., Mewes, M., Vallat, C., Witasse, O., and Altobelli, N.: Comparing observations of closely located JUICE and STEREO-A spacecraft during the widespread 13 May 2024 solar energetic particle event, Astronomy Astrophysics, 701, A13, https://doi.org/10.1051/0004-6361/202555301, 2025.

Roussos, E., Allanson, O., André, N., Bertucci, B., Branduardi-Raymont, G., Clark, G., Dialynas, K., Dandouras, I., Desai, R. T., Futaana, Y., Gkioulidou, M., Jones, G. H., Kollmann, P., Kotova, A., Kronberg, E. A., Krupp, N., Murakami, G., Nénon, Q., Nordheim, T., Palmaerts, B., Plainaki, C., Rae, J., Santos-Costa, D., Sarris, T., Shprits, Y., Sulaiman, A., Woodfield, E., Wu, X., and Yao, Z.: The in-situ exploration of Jupiter's radiation belts, Experimental Astronomy, 54, 745–789, https://doi.org/10.1007/s10686-021-09801-0, 2022.

Selesnick, R. S. and Albert, J. M.: Variability of the Proton Radiation Belt, Journal of Geophysical Research: Space Physics, 124, 5516–5527, https://doi.org/10.1029/2019JA026754, 2019.

Selesnick, R. S., Baker, D. N., Jaynes, A. N., Li, X., Kanekal, S. G., Hudson, M. K., and Kress, B. T.: Observations of the inner radiation belt: CRAND and trapped solar protons, Journal of Geophysical Research: Space Physics, 119, 6541–6552, https://doi.org/10.1002/2014JA020188, 2014.

Srour, J. R., Marshall, C. J., and Marshall, P. W.: Review of displacement damage effects in silicon devices, IEEE Trans. Nucl. Sci., 50, 653–670, https://doi.org/10.1109/TNS.2003.813197, 2003.

Tosi, F., Roatsch, T., Galli, A., et al.: Characterization of the Surfaces and Near-Surface Atmospheres of Ganymede, Europa and Callisto by JUICE, Space Science Reviews, 220, 2024.

Turner, D. L., O'Brien, T. P., Fennell, J. F., Claudepierre, S. G., Blake, J. B., Jaynes, A. N., Baker, D. N., Kanekal, S., Gkioulidou, M., Henderson, M. G., and Reeves, G. D.: Investigating the source of near-relativistic and relativistic electrons in Earth's inner radiation belt, Journal of Geophysical Research (Space Physics), 122, 695–710, https://doi.org/10.1002/2016JA023600, 2017.

Van Allen, J. A. et al.: Pioneer 11 observations of energetic particles in the Jovian magnetosphere, Science, 188, 459–462, https://doi.org/10.1126/science.188.4187.459, 1975.

Van Hoolst, T., Tobie, G., Vallat, C., Altobelli, N., Bruzzone, L., Cao, H., Dirkx, D., Genova, A., Gurvits, L. I., et al.: Geophysical Characterization of the Interiors of Ganymede, Callisto and Europa by ESA's JUpiter ICy moons Explorer, Space Science Reviews, 220, 44, https://doi.org/10.1007/s11214-024-01085-y, 2024.

Williams, D. J.: Energetic electron beams in Ganymede's magnetosphere, Journal of Geophysical Research, 109, A09 211, 2004.

https://doi.org/10.5194/egusphere-2026-2055
Preprint. Discussion started: 15 April 2026

Yuan, C. and Zong, Q.-G.: The double-belt outer radiation belt during CME- and CIR-driven geomagnetic storms, Journal of Geophysical Research: Space Physics, 118, 6291–6301, https://doi.org/10.1002/jgra.50564, 2013.